EVALUATION OF THE APPLICABILITY OF A TURBULENT WAKE INLET BOUNDARY CONDITION

P. A. Soliman[a], A. V. De Paula[b], A. P. Petry[a], and S. V. Möller[a]

Universidade Federal do Rio Grande do Sul
[b]Departamento de Engenharia Mecânica
[a]P. de Pós-Graduação em Engenharia Mecânica
Bairro Centro
CEP. 90050-170, Porto Alegre, RS, Brasil
paulo.soliman@ufrgs.br

Received: September 14, 2017
Revised: October 10, 2017
Accepted: November 01, 2017

ABSTRACT

With the objective of reducing the computational cost of the iterative processes of aerodynamic components design, tests were carried out to study under what conditions, and with what difference, only part of the calculation domain can be solved using as input information obtained from complete simulations already solved. An experimental study of an airfoil exposed to the wake interference of an upstream airfoil at a Reynolds number of 150,000 was used to verify the solutions of the Reynolds-Averaged Navier-Stokes equations solved applying the k-ω Shear Stress Transport model for turbulence closure. A Grid Convergence Index study was performed to verify if the solution of the equations for the adopted discretization leads to results within the asymptotic range. With the physical coherence of the numerical methodology verified, comparisons between the simulations with the domain comprising the two airfoils and the domain comprising only the downstream airfoil were performed. Computational time reductions in the order of 40% are observed. The differences in the aerodynamic coefficients for the two types of simulation are presented as a function of distances non-dimensionalized by the characteristic length of the body that disturbs the flow forming the wake, showing that the difference between the two methods was inversely proportional to the distance between the two bodies. Behavior that was maintained until a point where the simulation diverges, equivalent to 25% of the characteristic length of the body that generates the wake.

Keywords: computational fluid dynamics, tandem airfoils, wing design, grid convergence index, computational cost

NOMENCLATURE

t	time, s
u	velocity, m/s
$\bar{u}$	mean component of velocity, m/s
u'	fluctuating component of velocity, m/s
k	turbulent kinetic energy, m^2/s^2
G	turbulence production, m^2/s^3
Y	turbulence dissipation, m^2/s^3
S	user-defined source term
D	cross-diffusion term
C_ε	k-ε model constants
a^*	turbulence viscosity damper
F_2	SST model constant
a_1	SST model blending function
y^+	dimensionless wall distance
y_c	canard/wing vertical distance, m
d	canard/wing horizontal distance, m
c_c	canard chord, m
c_w	wing chord, m
Re	Reynolds number
y'	first prism layer height, m
u^*	friction velocity, m/s
C_D	aerodynamic drag coefficient
C_L	aerodynamic lift coefficient
r	refinement ratio
N	domain number of elements
D	domain number of dimensions
f	discrete solution of the parameter of interest
P	convergence order
w	GCI relaxation factor
P'	previous iteration value of P'
F_S	GCI safety factor
O_c	dimensionless offset
S'	dimensionless spacing

Greek symbols

ρ	density, kg/m^3
δ_{ij}	Kronecker delta
μ_t	turbulent viscosity, $N.s/m^2$
ε	turbulent kinetic energy dissipation rate, m^2/s^3
ω	specific turbulence dissipation rate, 1/s
Γ	effective diffusivity, $N.s/m^2$
σ	turbulent Prandtl number
δ	boundary layer thickness, m
ν	kinematic viscosity, m^2/s
ϵ	GCI relative error
β	GCI function

INTRODUCTION

The performance of a racing car airfoil is highly influenced by upstream disturbances (Soso and Wilson, 2006, Diasinos, 2014, Newbon et al., 2015). In a macro view, these perturbations alter the

magnitudes of the aerodynamic forces acting on the whole vehicle as well as their distribution, causing sudden changes in the dynamic behavior of the same (Perry and Marshall, 2008). This influence of an upstream body on the characteristics of the flow in the downstream body is not limited to motorsport vehicles: wind turbines (Breton et al., 2014), solar panels (Jubayer and Hangan, 2016), water turbines (Amiri et al., 2017), airfoils (Aziz and Mukherjee 2016, Merril and Peet, 2016) and various land vehicles (Watkins, 2008, Blocken and Toparlar, 2015, Blocken et al., 2016) are examples of subjects of previous studies. In the automobile case, the disturbances can be caused by the components of the car itself (Kim and Han, 2011, Dang et al., 2015). Several numerical optimization works of airfoils and its accessories (passive and active flow control devices, endplates) are found, but they look for optimal geometries for free flow conditions (Gopalarathnam and Selig, 1997, Amini et al., 2015, Wang et al., 2017). Other studies optimizes the geometries using domains that comprise the body of interest and the body that causes upstream perturbation. Physics are better reproduced but at a higher computational cost (Soliman et al., 2015, Iljaž et al., 2016). A solution used to reproduce the effects of the wake without having to solve the flow for the bodies upstream iteratively is to impose specific flow characteristics at the inlet of the domain (Newbon et al., 2015).

Although efficient from the computational point of view, imposing conditions in a certain region of the flow can intrinsically add errors to the numerical solution. This paper aims to clarify whether this technique is applicable on an industrial scale and, if so, under what conditions and with what precision in its calculations. It intends to assist any design or CAE (computer-aided engineering) engineer who deals with aerodynamic profiles operating under the influence of upstream bodies, deciding if and when to apply the technique to expedite design iterations. Even in large budget categories, such as Formula 1, there are limitations in the use of CFD (computational fluid dynamics), processing is limited in the number of double precision floating point operations (Fédération Internationale de L'Automobile, 2017), making the processing economy relevant even for these cases where powerful hardware is available.

To evaluate the technique an experimental work was reproduced via CFD. A study in which the body of interest was an airfoil with relative high camber, which has recurrent use in automobiles, subjected to wake interference from an upstream body led to the work of Michelsen and Mueller (1987). The behavior of the aerodynamic coefficients with the variation of the positioning between the bodies was reproduced through simulations with full domain and with only the downstream airfoil, imposing the wake at the inlet. Both were compared to the experimental data and to each other, resulting in relationships between differences in the results (associated with the technique) and dimensionless positioning of bodies.

THEORY

Although approaches such as LES and hybrids RANS/LES, like DES, already appear in the literature as applicable in the automotive industry (Ashton, 2016), the most applied modeling in these problems remains pure RANS with application of the Boussinesq hypothesis and a turbulence model for closing the equations (Toet, 2013).

Reynolds averaging consists in decompose variables into the mean and fluctuating components, for example the velocity components

$$u_i = \overline{u}_i + u'_i \tag{1}$$

applying Reynolds averaging in the continuity equation

$$\frac{\partial \rho}{\partial t} + \frac{\partial}{\partial x_i}\left(\rho u_i\right) = 0 \tag{2}$$

and in the momentum equation

$$\frac{\partial}{\partial t}\left(\rho u_i\right) + \frac{\partial}{\partial x_j}\left(\rho u_i u_j\right) = \frac{\partial p}{\partial x_i} + \frac{\partial}{\partial x_j}\left[\left(\frac{\partial u_i}{\partial x_i} + \frac{\partial u_j}{\partial x_i} - \frac{2}{3}\delta_{ij}\frac{\partial u_l}{\partial x_l}\right)\right] + \frac{\partial}{\partial x_j}\left(-\rho\overline{u'_i u'_j}\right) \tag{3}$$

applying the Boussinesq aproximation in the Reynolds stresses

$$-\rho\overline{u'_i u'_j} = \mu_t\left(\frac{\partial u_i}{\partial x_i} + \frac{\partial u_j}{\partial x_i}\right) - \frac{2}{3}\left(\rho k + \mu_t\frac{\partial u_k}{\partial x_k}\right)\delta_{ij} \tag{4}$$

Now, a method for calculating turbulent viscosity μ_t is required. There arise the approaches known as turbulence models. As there are several of these models, and many of them rely on empirical coefficients, there is no absolute model for all applications up to the present times. As the main focus of this paper is to serve for automotive applications, comparisons of turbulence models in the area have been revisited. Good results with the *k-ω* SST (Shear Stress Transport) model led to your choice (Ashton, 2016). The validity of this work for other areas already mentioned is not affected, since this is a widely accepted model in other fields as well.

The shear-stress transport *k-ω* was proposed by (Menter, 1994) to effectively blend the *k-ω* formulation (near-wall region) with *k-ε* (far field). The transport equations for k, ω and ε are

$$\frac{\partial}{\partial t}(\rho k)+\frac{\partial}{\partial x_i}(\rho k u_i)=\frac{\partial}{\partial x_j}\left[\Gamma_k \frac{\partial k}{\partial x_j}\right]+G_k-Y_k+S_k \quad (5)$$

$$\frac{\partial}{\partial t}(\rho \omega)+\frac{\partial}{\partial x_i}(\rho \omega u_i)=\frac{\partial}{\partial x_j}\left[\Gamma_\omega \frac{\partial \omega}{\partial x_j}\right]+G_\omega-Y_\omega+S_\omega \quad (6)$$

$$\frac{\partial}{\partial t}(\rho \varepsilon)+\frac{\partial}{\partial x_i}(\rho \varepsilon u_i)=\frac{\partial}{\partial x_j}$$
$$\left[\left(\mu+\frac{\mu_t}{\sigma_\varepsilon}\right)\frac{\partial \varepsilon}{\partial x_j}\right]+C_{1\varepsilon}\frac{\varepsilon}{k}(G_k+C_{3\varepsilon}G_b)-C_{2\varepsilon}\rho\frac{\varepsilon^2}{k}+S_\varepsilon \quad (7)$$

where G represents production, Γ the effective diffusivity, Y the dissipation due to turbulence, D the cross-diffusion term, S a user-defined source term, σ is the turbulent Prandtl number and $C_{1\varepsilon}$,$C_{2\varepsilon}$,$C_{3\varepsilon}$ are model constants. For more information on this treatment of turbulence, like the modeling of the effective diffusivity and the turbulence production and dissipation and the model constants, the reader is encouraged to read the works of Menter (1994), Wilcox (2006) and ANSYS® (2013). The turbulent viscosity is computed as

$$\mu_t=\frac{\rho k}{\omega}\frac{1}{\max\left[\frac{1}{a^*},\frac{SF_2}{a_1\omega}\right]} \quad (8)$$

where a^* is a turbulent viscosity damper that causes a low-Reynolds number correction, F_2 is a blending function and a_1 is a model constant. To treat the near-wall turbulent flow the implemented code applies methods to make the solution independent of y^+, the so-called Enhanced Wall Treatment. If the near-wall mesh is fine enough (y^+~1) it's considered able to solve the buffer layer and the viscous sublayer, if not a wall function based is applied. The use of EWT is recommended by the code developer, although making the solution more independent of y^+, careful with the mesh size close to the wall should be taken, as an unstructured grid will be applied prism layers must cover the entire thickness of the boundary layer (10-20 layers) and approximately 15 nodes should be located within it (ANSYS®, 2013). Details about how this was predicted and guaranteed in the creation of the mesh are presented in Geometry, Mesh and Boundary Conditions subsection. A finite volume method is then applied to solve the linear equation system formed by the integration of the governing equations on the individual control volumes of the computational grid. A second-order upwind scheme was applied for all the spatial discretizations with a pressure-based solver, pressure-velocity coupling was achieved using the segregated SIMPLE algorithm (Patankar, 1980). Constant under-relaxation factors were applied: 0.3 for pressure, 0.7 for momentum and 0.8 for turbulent kinetic energy and specific dissipation rate. Air was modeled as an incompressible fluid with a density equal to 1.23 kg/m^3 and a dynamic viscosity of 1.79x10^{-5} kg/m.s.

NUMERICAL METHODOLOGY

In this section, geometry, techniques for generating the meshes, their quality analysis adopted and boundary conditions will be explained. It is important to make it clear that the entire process from CAD (computer-aided design) to CFD post processing was done in a common workstation, equipped with 2 processors totaling 8 physical cores for parallel processing and 24 GB of ram. The intention was to use a representative machine of what is commonly available for design engineers, excluding cluster-based teams from top motorsport categories. The commercial code applied was ANSYS® Fluent 18.

Geometry, Mesh and Boundary Conditions

Geometry aimed to be as faithful as possible to the one described by Michelsen and Mueller (1987). The airfoil of interest is a Wortmann FX 63-137 with 0.152 m of chord, it has a maximum camber of 6% at 53.3% of the chord and a maximum thickness of 13.7% at 30.9% of the chord. The upstream body, responsible for causing the wake, employs the same profile however with 0.1 m of chord. From now on the airfoil of interest, where the coefficients were evaluated, will be called only by wing and the one located upstream only by canard, to coincide with the nomenclature of Michelsen and Mueller (1987). In the present work the angles of attack used were fixed, being the largest found in the reference experimental work. Figure 1 shows a 2D view of the canard and wing and also the most relevant dimensions for this study, the distance y_c is measured from the quarter chord position of each profile, d is the distance between the canard trailing edge and the wing leading edge.

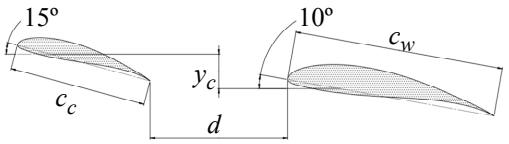

Figure 1. Geometries and distances.

Although the experimental work aims to obtain the two-dimensional aerodynamic coefficients, for the dimensions of the tunnel in question three-dimensional effects are unavoidable, as described by Mueller and Jansen (1982). Indeed, initial simulations performed to obtain 2D coefficients did not show agreement with the experimental ones. One technique employed by the authors to reduce 3D effects was the use of endplates in the wing. This was done since its span, 0.41 m, does not extend through the whole section of the tunnel, unlike the canard. This

configuration, wing plus endplate, was used for its better representation of the experiment. Besides it is interesting its use in a work that can serve as benchmarking for automotive applications, since the vast majority of the wings for this purpose make use of endplates to reduce aerodynamic losses due to 3D effects, like wingtip vortices (Katz, 1995, McBeath, 2006).

To consider the blocking effect of the experimental work, the cross section of the domain is the same of the wind tunnel where the experiment was conducted. To avoid modeling the inlet contraction cone before the test section and the diffuser after, the domain extended 10 times the wing chord upstream from the canard leading edge and 15 times the wing chord downstream from the wing trailing edge. So the boundary layer was solved only for the test section walls and for the wing, canard and endplate. The computational domain and the boundary conditions are illustrated in Fig. 2, dimensions in meters.

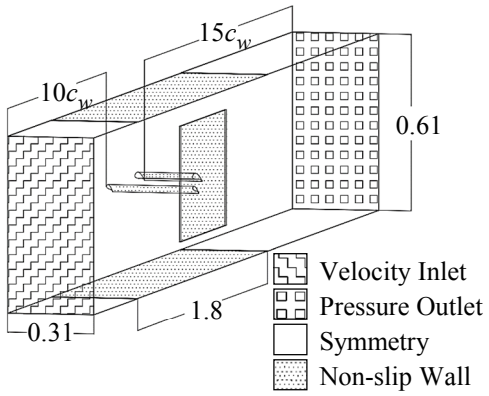

Figure 2. Computational domain and boundary conditions.

At the velocity inlet a magnitude of 15 m/s was prescribed, normal to the plane, resulting in a Reynolds number of 150000, and a turbulence intensity of 0.1% corresponding to the wind tunnel conditions of the experimental work. For each case, planes located in $d/2$ were created in the post-processing of the simulations with the complete domain already solved, from it profiles of x, y and z velocity, turbulent kinetic energy k and the specific dissipation rate ω were exported. These profiles were used as inlets for the cases with only the wing. The domain for such cases has its inlet plane in the exact location of the plane where the profiles were exported, the remaining dimensions were retained. This process is illustrated in Fig. 3 and Fig. 4. The velocity contours were plotted in the central symmetry plane and the flow is developing from left to right, conditions that will be maintained in plots presented throughout the work. The plane in which the variables are sampled intercepts the endplate, as shown in Fig. 4.

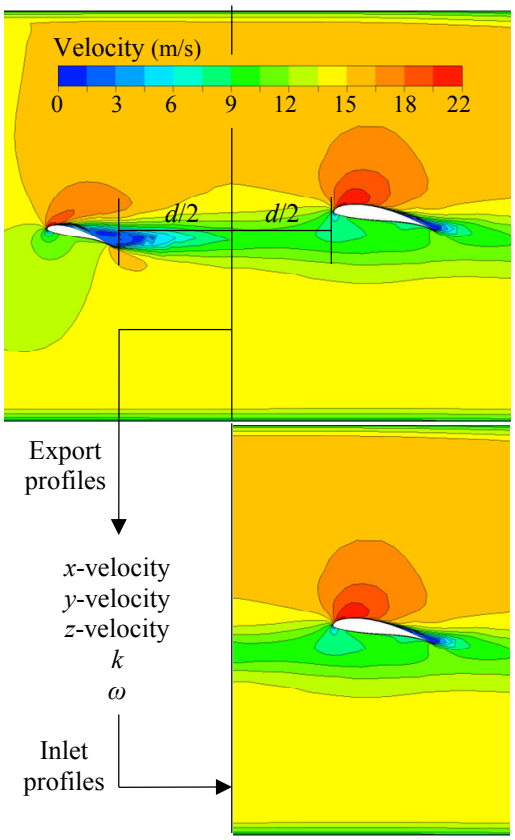

Figure 3. Profile plane as inlet boundary condition.

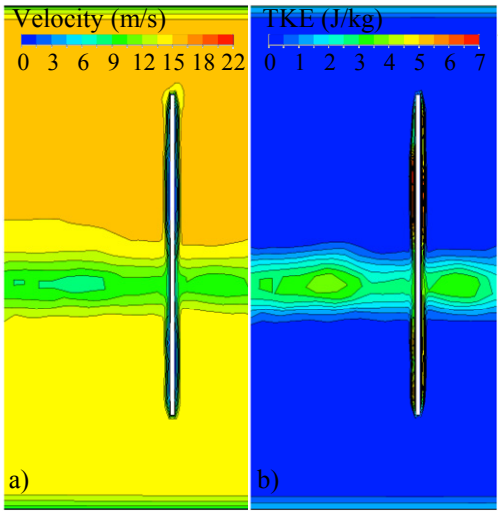

Figure 4. Exported planes examples, a) x-velocity b) turbulent kinetic energy.

The domain was discretized with tetrahedral cells and prism layers in the near wall region. Although the EWT allows the SST solution for higher values of y^+ (as seen in Theory section), solving the entire boundary layer is still recommended for better results with this turbulence model (Diasinos, 2014). It was then necessary to ensure that 20 prisms cover the boundary layer (also in Theory section) and y^+~1. For this it is necessary

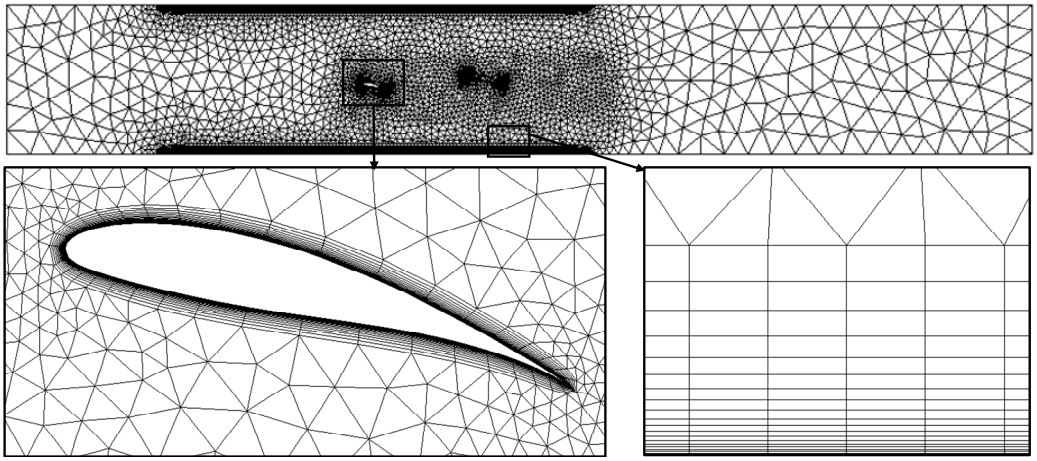

Figure 5. Mesh example (zoom boxes are on the same scale).

to estimate the boundary layer thickness and the height required for the first layer of prisms. To simplify this process, the one-seventh-power law for flat plate turbulent boundary layer was used (Çengel and Cimbala, 2014).

$$\frac{\delta}{x} = \frac{0.16}{Re^{1/7}} \tag{9}$$

and the height of the first layer of prisms comes from the definition of y^+

$$y^+ = \frac{y' u_*}{\nu} \tag{10}$$

as the length x varies for the walls, prism layers with different dimensions were required for the canard, wing, endplate and tunnel section. An illustration of the result of this approach is presented in the Fig. 5. Figure 6 shows how y^+ remained close to the desired range. At the intersection wing/endplate some cells reached slightly higher values, but still below 5, which is acceptable (ANSYS®, 2006). The convergence criteria adopted was residuals below 10^{-5} with the stabilization of C_D and C_L, conditions that were typically met with 1500-2000 iterations.

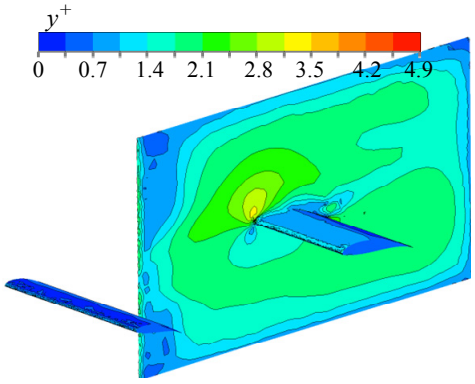

Figure 6. Contours of wall y^+.

Grid Convergence Index

To verify the quality of the meshes, the GCI method proposed by Roache (1994) was selected. The choice was motivated by being a standardized method of quantification of the uncertainties associated to the refinements of the meshes, which is accepted and has already been used in several previous works (Cheng et al., 2011, Diasinos, 2014, Fintelman et al., 2015, Shim et al., 2017). The methodology derives from the generalized Richardson Extrapolation, in the present work the version of GCI applied compares three successive refinements in mesh. The equations involved in this section can be found in the format presented in the texts of Roache (1994 and 1997). As the meshes used are unstructured, the ratio of refinement r between them is neither constant nor directly obtained, for its calculation it is used

$$r_{ij} = \frac{N_i^{1/D}}{N_j} \tag{11}$$

where the index i indicates the most refined mesh and the index j the least refined, N is the number of elements in the domain and D is the number of dimensions, 3 in this case. The relative error between two meshes is calculated

$$\epsilon_{ij} = \frac{f_j - f_i}{f_i} \tag{12}$$

where f is the discrete solution of the parameter of interest, for this study C_D was selected as f. One can then calculate the convergence order P with simple substitution iteration with a relaxation factor w equal to 0.5 and P' equals to the previous iterate value of P, starting with an initial guess of 2. The iteration equation is

$$P = wP' + (1-w)\frac{\ln\beta}{\ln r_{12}} \quad (13)$$

where β is obtained from

$$\beta = \frac{(r_{12}{}^{P} - 1)\in_{23}}{(r_{23}{}^{P} - 1)\in_{12}} \quad (14)$$

finally the GCIs for the fine and coarse mesh can be calculated:

$$GCI_{12} = F_S|\in_{12}|(r_{12}{}^{P} - 1) \quad (15)$$

$$GCI_{23} = F_S|\in_{23}|(r_{23}{}^{P} - 1) \quad (16)$$

where F_S is the safety factor, the asymptotic range is considered achieved when $GCI_{23} \approx r_{12}{}^{P} GCI_{12}$.

A coarse ($1.1\text{x}10^6$ cells), a medium ($3.3\text{x}10^6$ cells), and a fine mesh ($9.7\text{x}10^6$ cells) were generated for the same case. Applying a conservative safety factor of 3 a GCI_{23} of 6.5% and a GCI_{12} of 5.1% were obtained, as $GCI_{23}/(r_{12}{}^{P}\ GCI_{12})$=1.13 the asymptotic range was considered achieved. The coarse mesh was chosen because it presents a *GCI* close to the fine mesh but with a considerable reduction in computation time.

RESULTS AND DISCUSSION

The results are presented in two sections following the logical order of the study. First, the canard/wing spacing is fixed and the offset is varied between values such as the experimental work of Michelsen and Mueller (1987). Simulations with the whole domain and only with the wing were made and compared with the experimental values in order to verify the two numerical methodologies, these results are presented in the first subsection of this section.

After this first study, the offset was fixed and the spacing gradually reduced, to seek the minimum distance that is feasible to export the profiles and simulate only the wing in the domain. As experimental data for the spacing values tested are not available, comparisons were made between full domain and only wing simulations. These results are presented in the second subsection of this section.

The studied parameters were nondimensionalized by the characteristic length of the body that disturbs the flow in order to generate the wake, in this case the canard chord. The dimensionless offset is defined as

$$O_c = \frac{y_c}{c_c} \quad (17)$$

and the dimensionless spacing

$$S' = \frac{d}{c_c} \quad (18)$$

It is important to clarify that the dimensionless S' is not equal to the S originally presented by Michelsen and Mueller (1987). This change was necessary due to the different spacing values studied in the present work.

The difference between coefficients calculated by the full domain and only the wing simulations is defined as

$$\Delta C_i = |C_{if} - C_{iw}| \quad (19)$$

Where the sub index i is replaced by L for lift or D for drag, and the sub indexes f and w represents simulations with full domain and only the wing respectively.

Full-domain simulations took on average 57 minutes of wall-clock time to run 2000 iterations while those with just the wing took on average 31 minutes. No changes were observed in the number of iterations required to reach the convergence criteria between the two methods. This decrease is explained by the approximately 30% reduction in the number of cells in the domain.

Dimensionless Offset Effect

The main objective of this subsection is to verify the consistency of the results for C_L and C_D when compared with the experimental ones. In addition, it was possible to check if there is influence of the offset on the difference of simulations with full domain or only the wing, S' was fixed in 3.4 and for O_C were tested: -0.75; -0.5; -0.25; 0; 0.25; 0.5 and 0.75. Figure 7 shows two tested configurations and their effect on velocity contours on the central symmetry plane.

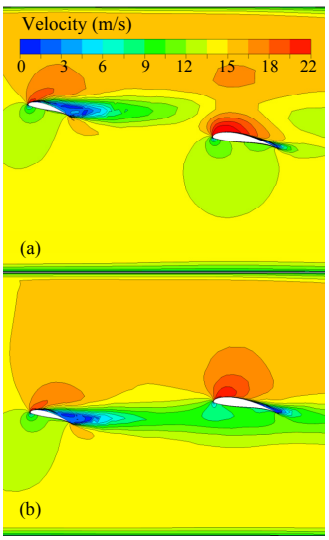

Figure 7. Offset effect, a)O_c=0.75 b)O_c=-0.25.

Figure 9 presents graphs of C_L and C_D varying with O_C. The error bars of the experimental work are based on studies of uncertainties of Mueller (1982 and 1986) for the same wind tunnel and flow conditions, as suggested by the author. The error bars of the present work are based on GCI. Figure 8 shows the difference found between the two simulation methods for the aerodynamic coefficients.

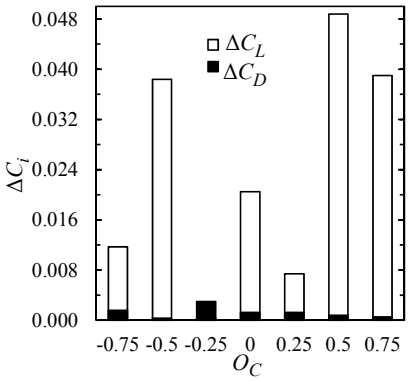

Figure 8. Difference between coefficients obtained from both numerical methods versus dimensionless offset.

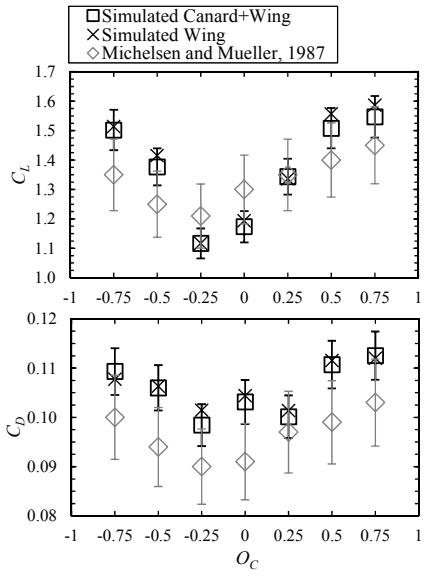

Figure 9. Aerodynamic coefficients vs. dimensionless offset.

Comparing the experimental and numerical results first, the correct capture of the trends is observed as the graph of Fig. 9 shows, although considerable quantitative differences are found for some points, all remained within the ranges of uncertainties. The result was considered satisfactory for the present study, and the simulations able to serve as comparative between the two numerical methodologies.

Observing Fig. 8, it can be seen that the largest differences in C_L and C_D occur for different O_C values, and a trend is not observed.

Dimensionless Spacing Effect

This subsection aims to study how closely the geometry of interest can be of the one that disturbs the flow so that the methodology of wake imposition can be applied, and the differences. To facilitate comparison with other cases, this distance was nondimensionalized with the characteristic length of the disturbing body, as already presented. The O_c was fixed in 0.25 and for S' were tested: 0.25; 0.5; 1; 1.5; 2; 2.5; 3 and 3.4.

In an analogous way to that shown in the previous subsection, Fig. 10 shows symmetry plane velocity contours for two different spacings tested, Fig. 11 presents graphs of C_L and C_D varying with S' and Fig. 12 shows the difference found between the two simulation methods.

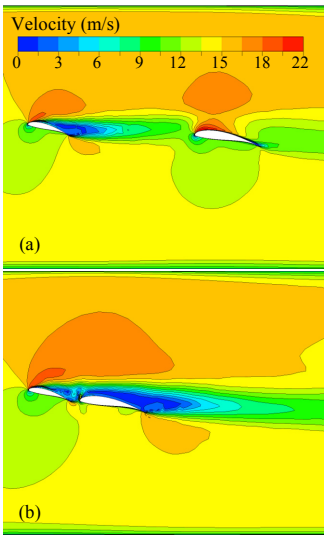

Figure 10. Spacing effect, a)S'=3 b)S'=0.25.

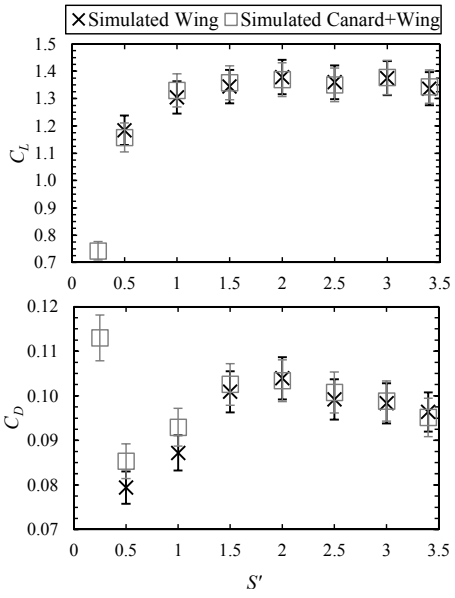

Figure 11. Aerodynamic coefficients vs. dimensionless spacing.

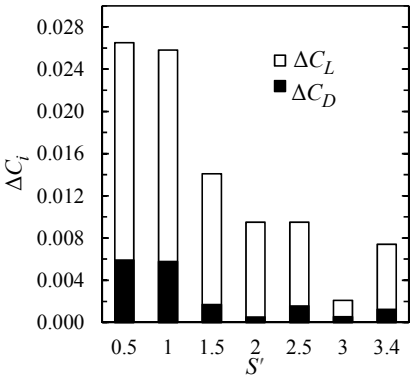

Figure 12. Difference between coefficients obtained from both numerical methods versus dimensionless offset.

Analyzing Figs. 10 and 11 it is noted that the aerodynamic coefficients decreases as the *S'* is reduced. This behavior is expected since the reduction of *S'* means that the wing is entering further into the wake of the canard, exposed then to greater velocity deficit. The increase in C_D at S'=0.25 is explained because in this condition the boundary layer of the wing is separated along its entire upper surface, causing considerable increase in pressure drag.

Figure 12 shows that the difference between the two numerical methodologies increases with the decrease of *S'*, this behavior continues until S'=0.25, when the simulation diverges and therefore results are not presented for this condition in Figs. 11 and 12.

CONCLUSIONS

The purpose of this numerical study was to determine whether a wake from an upstream body can be used as inlet condition of the flow on an airfoil in order to simplify the numerical analysis and reduce computational costs.

From the general analysis of the work it is first concluded that the numerical methodology described was successful in reproducing the experimental work within the study proposals. Also, that the partial solution of the domain obtained results that are consistent with the simulation of the full domain, with graphically expressed differences.

With respect to the influence of the offset on the difference of the results, a clear trend was not noticed and a study with more variations in the offset values is necessary to conclude if this dependence exists. The influence of the spacing was clear with differences increasing gradually up to a distance equivalent to 25% of the characteristic length of the body that generates the wake, when the simulation diverges. The differences for the other spacings can serve as an initial guide to encourage or not the use of this methodology to reduce computational cost, depending on the application. Regarding the computational cost, a 45% wall-clock time drop was observed to run 2000 iterations in the comparison between complete domain and only with the wing. This fact is directly explained by the reduction of approximately 30% in the number of cells.

ACKNOWLEDGEMENTS

This work was conducted during a scholarship supported by CAPES at the Federal University of Rio Grande do Sul. Financed by CAPES – Brazilian Federal Agency for Support and Evaluation of Graduate Education within the Ministry of Education of Brazil. The Corresponding Author of this paper wishes to express his gratitude for the scholarship provided by CAPES.

REFERENCES

Amini, Y., Emdad, H., and Farid, M., 2015, Adjoint shape optimization of airfoils with attached Gurney Flap, Aerospace Science and Technology, Vol. 41, pp. 216-228.

Amiri, K., Mulu, B., Raisee, M., and Cervantes, M. J., 2017, Effects of Upstream Flow Conditions on Runner Pressure Fluctuations, Journal of Applied Fluid Mechanics, Vol. 10, No. 4, pp. 1045-1059.

ANSYS®, 2013, *Fluent 15.0 Theory Guide,* ANSYS®, Inc.

ANSYS®, 2006, *Fluent 6.3 User's Guide,* ANSYS®, Inc.

Ashton, N., West, A., Lardeau, S., and Revell, A., 2016, Assessment of RANS and DES Methods for Realistic Automotive Models, Computers and Fluids, Vol. 128, pp. 1-15.

Aziz, H., and Mukherjee, R., 2016, Vortex Interaction and Roll-Up in Unsteady Flow past Tandem Airfoils, Journal of Applied Fluid Mechanics Vol. 9, No. 6, pp. 3087-3100.

Blocken, B., and Toparlar, Y., 2015, A Following car Influences Cyclist Drag: CFD Simulations and Wind Tunnel Measurements, Journal of Wind Engineering and Industrial Aerodynamics, Vol. 145, pp. 178-186.

Blocken, B., Toparlar, Y., and Andrianne, T., 2016, Aerodynamic Benefit for a Cyclist by a Following Motorcycle, Journal of Wind Engineering and Industrial Aerodynamics, Vol. 155, pp. 1-10.

Breton, S.-P., Nilsson, K., Olivares-Espinosa, H., Masson, C., Dufresne, L., and Ivanell, S., 2014, Study of the Influence of Imposed Turbulence on the Asymptotic Wake Deficit in a Very Long Line of Wind Turbines, Renewable Energy, Vol. 70, pp. 153-163.

Çengel, Y. A., Cimbala, J. M., 2014, *Fluid Mechanics: Fundamentals and Applications*. McGraw-Hill Book Company.

Cheng, S. Y., Tsubokura, M., Nakashima, T., Nouzawa, T., and Okada, Y., 2011, A Numerical Analysis of Transient Flow Past Road Vehicles

Subjected to Pitching Oscillation, Journal of Wind Engineering and Industrial Aerodynamics, Vol. 99, No. 5, pp. 511-522.

Dang, T. P., Gu, Z., and Chen, Z., 2015, Numerical Simulation of the Flow Field Around the Race Car in Case: Stationary Wheel and Rotating Wheels, International Journal of Numerical Methods for Heat and Fluid Flow, Vol. 25, No. 8, pp. 1896-1911.

Diasinos, S., Keogh, J., and Doig, G., 2014, Flow Compressibility Effects Around an Open-Wheel Racing Car, The Aeronautical Journal, Vol. 118, No. 1210, pp. 1409-1431.

Fédération Internationale de L'Automobile, 2017, *Formula One Sporting Regulations*.

Fintelman, D. M., Hemida, H., Sterling, M., and Li, F.-X., 2015, CFD Simulations of the Flow Around a Cyclist Subjected to Crosswinds, Journal of Wind Engineering and Industrial Aerodynamics, Vol. 144, pp. 31-41.

Gopalarathnam, A., Selig, M., and Hsu, F., 1997, Design of High-Lift Airfoils for Low Aspect Ratio Wings with Endplates, in: *15th Applied Aerodynamics Conference.*

Iljaž, J., Škerget, L., Štrakl, M., and Marn, J., 2016, Optimization of SAE Formula Rear Wing, Strojniški Vestnik - Journal of Mechanical Engineering, Vol. 62, No. 5, pp. 263-272.

Jubayer, C. M., and Hangan, H., 2016, A Numerical Approach to the Investigation of Wind Loading on an Array of Ground Mounted Solar Photovoltaic (PV) Panels, Journal of Wind Engineering and Industrial Aerodynamics, Vol. 153, pp. 60-70.

Katz, J., 1995, *Race Car Aerodynamics: Designing for Speed*, Bentley Publishers.

Kim, J-H., and Han Y. O., 2011, Experimental Investigation of Wake Structure Around an External Rear view Mirror of a Passenger Car, Journal of Wind Engineering and Industrial Aerodynamics, Vol. 99, pp. 1197-1206.

McBeath, S., 2006, *Competition Car Aerodynamics*, Haynes Publishing.

Menter, F. R., 1994, Two-Equation Eddy-Viscosity Turbulence Models for Engineering Applications, AIAA Journal, Vol. 32, No. 8, pp. 1598-1605.

Merril, B. E., and Peet, Y., 2016, Effects of Upstream Disturbances on a Pitching NACA0012 Airfoil, in: *54th AIAA Aerospace Sciences Meeting.*

Michelsen, W. D., and Mueller, T., 1987, Low Reynolds Number Airfoil Performance Subjected to Wake Interference from an Upstream Airfoil, in: *5th Applied Aerodynamics Conference.*

Mueller, T. J., and Jansen, B. J., 1982, Aerodynamic Measurements at Low Reynolds Numbers, in: *12th Aerodynamic Testing Conference*.

Mueller, T. J., and Jansen, B. J., 1986, Low Reynolds Number Wind Tunnel Measurements: The Importance of Being Earnest, in: *Aerodynamics at Low Reynolds Numbers $10^4<Re<10^6$ International Conference.*

Newbon, J., Dominy, R., and Sims-Williams, D., 2015, CFD Investigation of the Effect of the Salient Flow Features in the Wake of a Generic Open-Wheel Race Car, SAE International Journal of Passenger Cars - Mechanical Systems, Vol. 8, No. 1, pp. 217-232.

Patankar, S. V., 1980, *Numerical Heat Transfer and Fluid Flow*, Hemisphere Publishing.

Perry, R., and Marshall, D., 2008, An Evaluation of Proposed Formula 1 Aerodynamic Regulations Changes Using Computational Fluid Dynamics, in: *26th AIAA Applied Aerodynamics Conference.*

Roache, P. J., 1994, Perspective: A Method for Uniform Reporting of Grid Refinement Studies, Journal of Fluids Engineering, Vol. 116, No. 3, pp. 405.

Roache, P. J., 1997, Quantification of Uncertainty in Computational Fluid Dynamics, Annual Review of Fluid Mechanics, Vol. 29, No. 1, pp. 123-160.

Shim, H.-S., Lee, Y.-N., and Kim, K.-Y., 2017, Optimization of Bobsleigh Bumper Shape to Reduce Aerodynamic Drag, Journal of Wind Engineering and Industrial Aerodynamics, Vol. 164, pp. 108-118.

Soliman, P. A., Martins, M. E. S., Schommer, A, 2015, Formula SAE Aerodynamics: Design Process with Focus on Drivability, in: *24th SAE Brazil International Congress and Display.*

Soso, M. D., and Wilson, P. A., 2006, Aerodynamics of a Wing in Ground Effect in Generic Racing Car Wake Flows, Proceedings of the Institution of Mechanical Engineers, Part D: Journal of Automobile Engineering, Vol. 220, No. 1, pp. 1-13.

Toet, W., 2013, Aerodynamics and Aerodynamic Research in Formula 1, The Aeronautical Journal Vol. 117, No. 1187, pp. 1-26.

Wang, H., Bai, Q., Hao, X., Hua, L., and Meng, Z., 2017, Genetic Algorithm-Based optimization Design Method of the Formula SAE Racing Car's Rear Wing, Proceedings of the Institution of Mechanical Engineers, Part C: Journal of Mechanical Engineering Science, Vol. 0, No. 0, pp. 1-15.

Watkins, S., and Vino, G., 2008, The effect of Vehicle Spacing on the Aerodynamics of a Representative Car Shape, Journal of Wind Engineering and Industrial Aerodynamics, Vol. 96, No. 6-7, pp. 1232-1239.

Wilcox, D. C., 2006, *Turbulence Modeling for CFD*, DCW Industries.